Supplementary Materials

Constructing dendrite-suppressing separator based on cellulose acetate and polyoxometalates toward uniform lithium electrodeposition

Xiyue Zhang, Jiayuan Zhang, Gui Wang, Chunhui Zhang, Linlin Fan*, Yundong Cao, Hong Liu, Guanggang Gao*

School of Materials Science and Engineering, University of Jinan, Jinan 250022, China

*Corresponding authors

E-mail: mse_fanll@ujn.edu.cn (Linlin Fan); mse_gaogg@ujn.edu.cn (Guanggang Gao)

Experimental section

Preparation of CA separator and CA/PMo_{12} separator

Cellulose acetate (CA) and PMo_{12} are dissolved in DMF solution at a certain proportion under stirring at 75 °C. The CA/PMo_{12} separator is prepared through the blade coating technology on glass substrate, and then it is soaked in a mixture of H_2O and ethanol (v: v=1: 1) for coagulation bath (4 °C for 2 h). The peeled CA/PMo_{12} separator is dried at 70 °C and cut into 20 mm discs for cell assembly. As a comparison, CA separator was prepared via same approach without PMo_{12}.

Preparation of $LiFePO_4$ cathode

The $LiFePO_4$ electrode was produced by mixing $LiFePO_4$, Super P, and PVDF in a weight ratio of 80%:10%:10% and dissolving in NMP to form a slurry, which was then coated on Al foil and dried in a vacuum oven at 60 °C for 24 h. Afterwards, the electrodes were punched into 10 mm disks in diameter, and the areal loading of $LiFePO_4$ was about 1.08 mg cm^{-2}.

Chemical reagents and materials

All the chemicals obtained from the supplier were used directly without further purification. All solvents were analytical grade reagents. N, N-dimethylformamide (DMF) and $H_3PMo_{12}O_{40}{\cdot}xH_2O$ (PMo_{12}) were purchased from Sinopharm Chemical Reagent Co., Ltd. Cellulose acetate (acetyl content ~32.0 %, hydroxyl content ~8.7 %) was purchased from Shanghai Macklin Biochemical Technology Co., Ltd. $LiFePO_4$ was bought from Kelude Experimental Equipment Technology Co., Ltd.

Materials characterization

The microstructures and elemental mappings of separators were obtained via scanning electron microscope (SEM, Zeiss, Gemini 300) with energy dispersive spectrometer (EDS, Oxford, X-Max^N 50). X-ray diffraction (XRD) was detected by Rigaku

SmartLab 9KW. X-ray photoelectron spectroscopy (XPS) was recorded on an ESCA Lab MKII X-ray photoelectron spectrometer with non-monochromatized Mg Kα X-rays as the excitation source. Fourier transform infrared spectroscopy (FTIR) was obtained using a NEXUS-870 spectrophotometer with KBr pellets. Contact angles were detected by a POWEREACH JC2000D2G instrument. The specific surface area of samples was determined by the Brunauer-Emmett-Teller (BET) nitrogen adsorption/desorption method (Autosorb-iQ-MP, Quantachrome). In-situ optical microscopy studies of Li//Li symmetrical cells were performed in transparent glass cell (Beijing Scistar Technology Co., Ltd.) viewed by an optical microscopy. Ultraviolet-visible (UV-Vis) measurement was performed by SHIMADZU UV-3600 spectrometer within the wavelength range of 200-600 nm. Raman test was carried out by a Raman spectrometer (Labramis, Horiba Jobbin Yvon, Paris, France) with wavelength of 532 nm. A universal material testing machine (CMT6103/ZWICK/Instron 5969) was utilized to test the mechanical properties of separator.

Electrochemical measurement

The CR2032-type coin cells were used to test Li//Li symmetrical cells and $LiFePO_4$//Li cells. 1.0 M $LiPF_6$ dissolved in DMC: EC: DME = 1: 1: 1 vol% with 10% FEC and 2% VC solvent was applied as the electrolyte. Cyclic voltammetry (CV) measurements were performed between 3.0 and 4.2 V via a DH7003 electrochemical workstation (Jiangsu Donghua Analytical Instrument Co., Ltd., China), which was also used to record electrochemical impedance spectroscopy (EIS) of cells with a potential amplitude of 5 mV and frequency ranging from 100 kHz to 0.01 Hz. The cycle performance test was carried out on the Neware battery test system (CT-4008-Tn-5V10mA-164, Shenzhen Neware Electronics Co., Ltd., China).

The electrolyte uptake test

The electrolyte uptake of the separator was calculated using equation:

$$\text{Electrolyte uptake (\%)} = \frac{\Delta w}{w_0} \times 100\% \quad (1)$$

where Δw is the weight difference of the separator after and before the immersion in the electrolytes for 1 h, and w_0 is the original weight of the separator.

Ionic conductivity test

The ionic conductivity (σ) of the electrolyte-soaked separators was evaluated with two stainless steel (SS) blocking cells (SS//separator//SS) by testing the EIS in the frequency range from 1000 kHz to 0.01 Hz on the electrochemical workstation. The ionic conductivity was calculated according to the following equation:

$$\sigma = \frac{D}{R_b \times S} \quad (2)$$

where D is the thickness of the separator, R_b and S represent the bulk resistance and the effective area of the separator, respectively.

Lithium ion transference number test

The lithium ion transference number was measured by sandwiching the separators between two lithium metal electrodes using electrochemical working station. R_0 and R_s refer to the interfacial resistance before and after AC impedance. I_0 and I_s represent the current value in initial and steady state under a polarization potential of 10 mV. t_{Li^+} is the lithium transfer number, and the value is calculated according to the following Bruce-Vincent-Evans equation:

$$t_{Li+} = \frac{I_s(\Delta V - I_0 R_0)}{I_0(\Delta V - I_s R_s)} \quad (3)$$

DFT calculations

The calculations were performed within the framework of DFT, by using the projector augmented wave method as implemented in the Vienna ab Initio Simulation Package. The exchange-correlation energy was in the form of Perdew-Bruke-Ernzerhof. The cutoff energy for the plane-wave basis set was 500 eV, and 2×2×1 Γ-centered k-point grids were used for the Brillouin zone integrations. For the surface systems, the bottom atom layers were fixed to simulate the body state, while the top atom layers were free to simulate the surface state. To reduce the interactions between each surface, a vacuum of 20 Å was contained in our calculation models. All structures were fully relaxed to the optimized geometry with the force convergence set at 0.01 eV/Å. To investigate the lowest energy configurations of adsorbed systems, we carefully manipulated structure parameters of the initial state (the distance, angle, and displacement between molecule and surface) to fully relax and selected the lowest energy result as the final state. The binding energy (E_{ads}) of lithium adsorbing on the CA and CA/PMo_{12} are calculated referring to the following equation:

$$E_{ads} = E_{total} - E_a - E_{Li}$$

where E_{total} is the total energy of CA and CA/PMo_{12} combined with lithium, E_a is the surface energy of CA and CA/PMo_{12}, and E_{Li} represents the energy of lithium in vacuum.

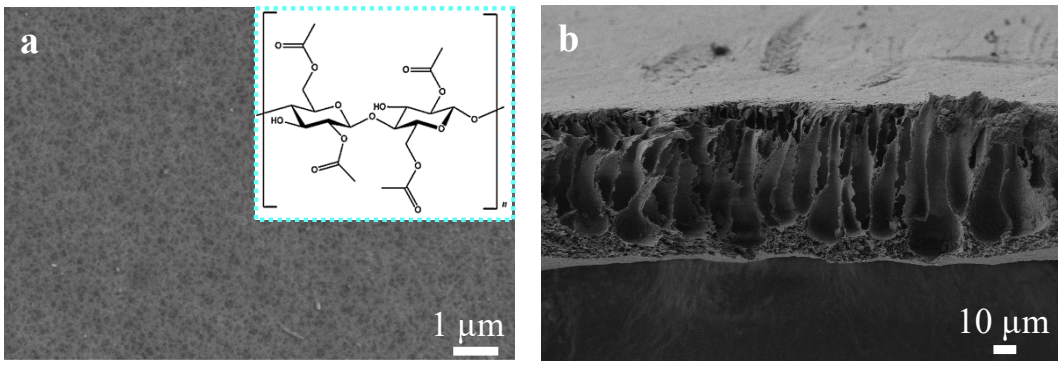

Fig. S1 (a) The top surface SEM image (inset: molecular formula of CA) and (b) cross section SEM image of CA separator.

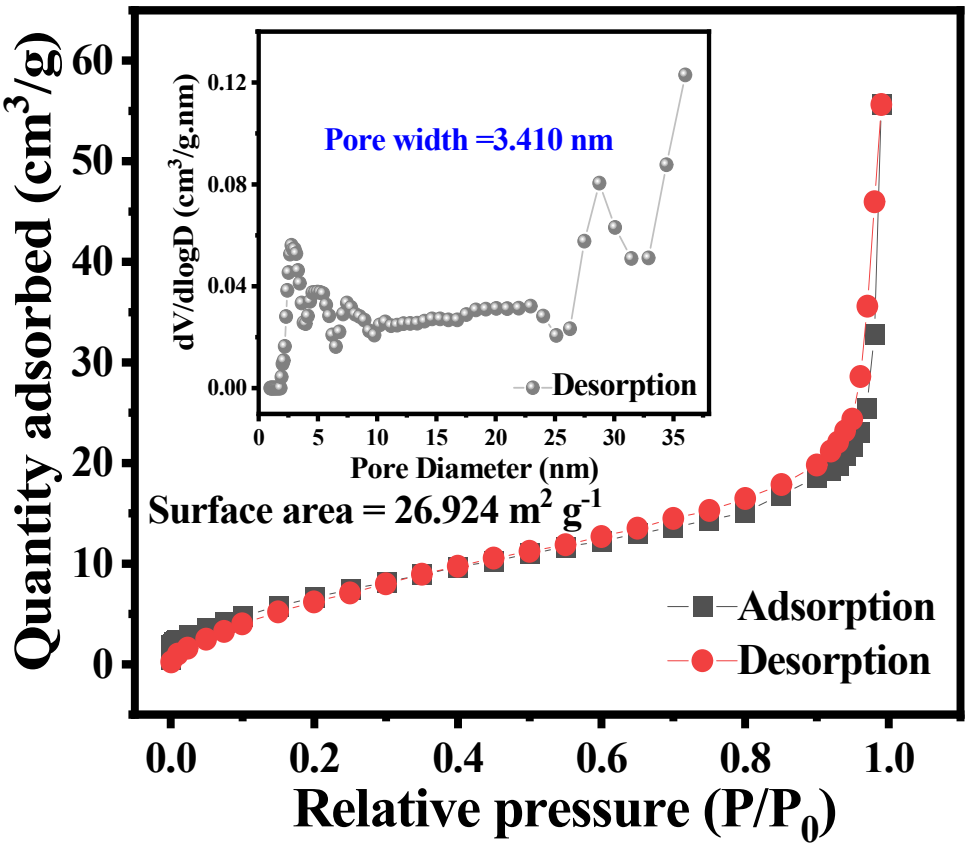

Fig. S2 N_2 sorption isotherm and related pore size distribution of CA separator.

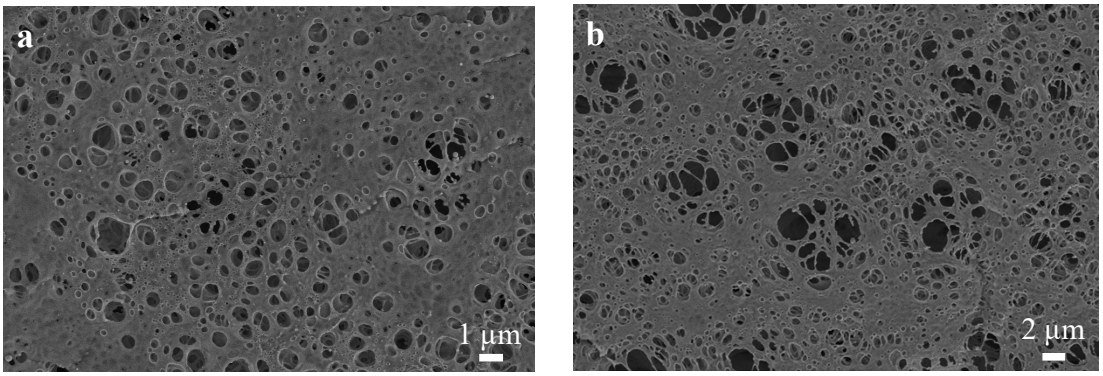

Fig. S3 SEM images of CA/PMo_{12} separators with PMo_{12} dosage of 0.1 mM (a) and 0.3 mM (b), respectively.

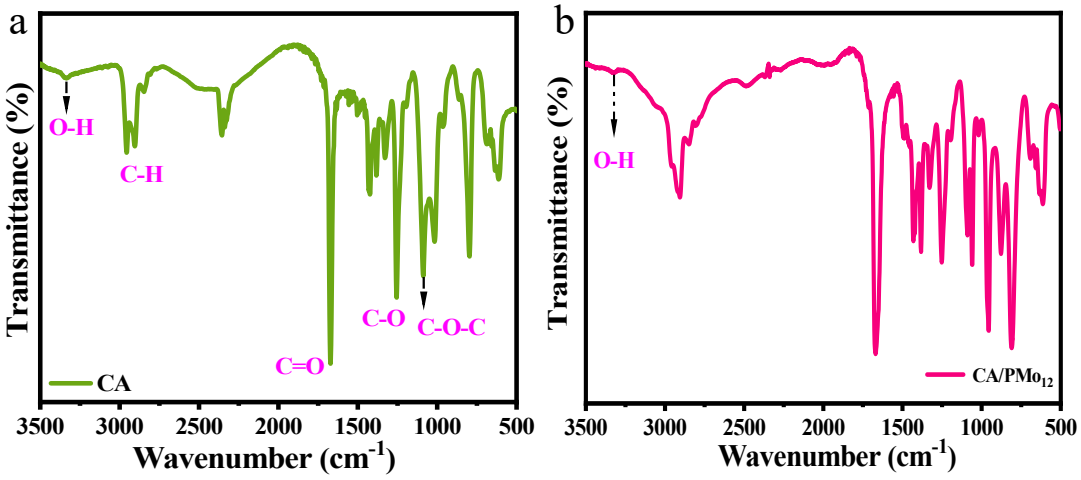

Fig. S4 FTIR spectra of (a) CA separator and (b) CA/PMo_{12} separator.

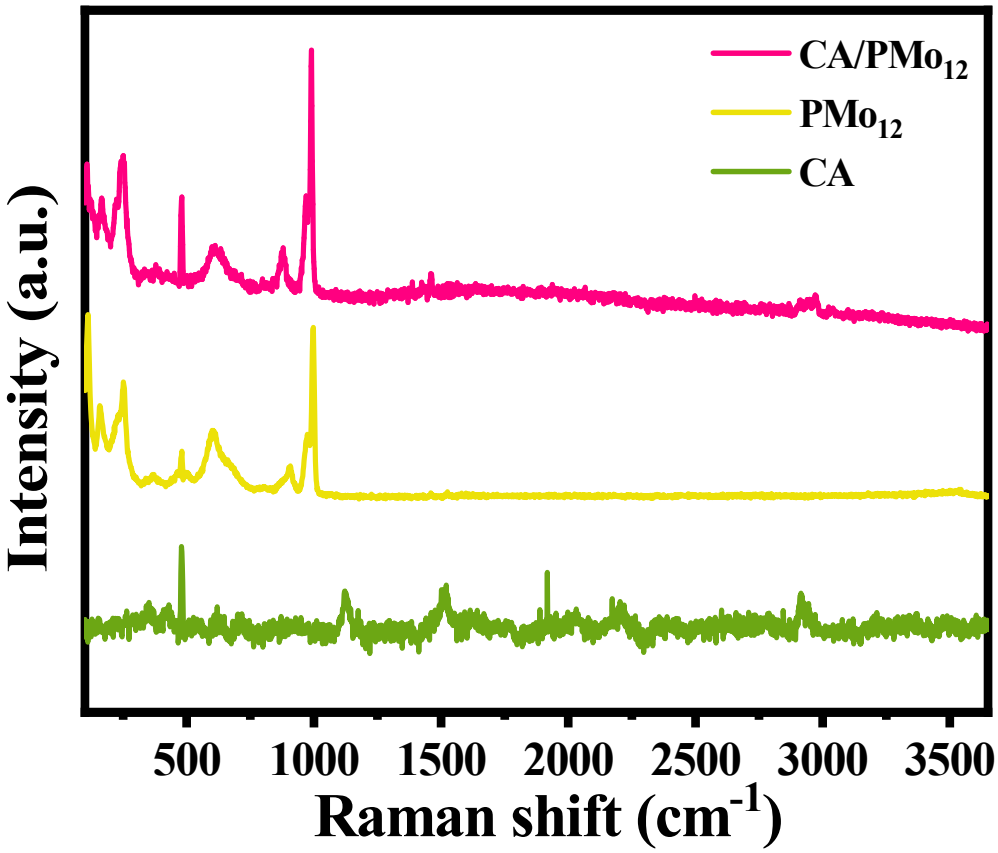

Fig. S5 Raman spectra of PMo_{12} powder, CA separator, and CA/PMo_{12} separator.

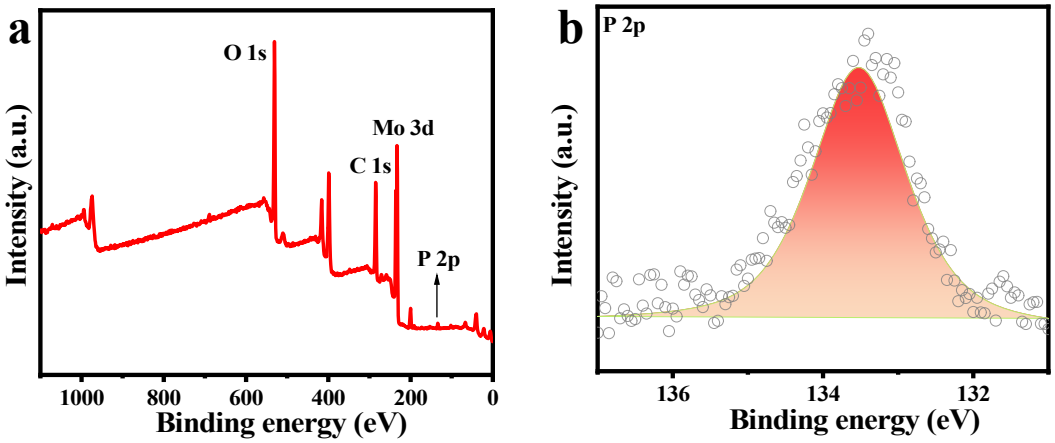

Fig. S6 XPS analysis of CA/PMo_{12} separator: (a) the survey spectra and (b) P 2p spectra.

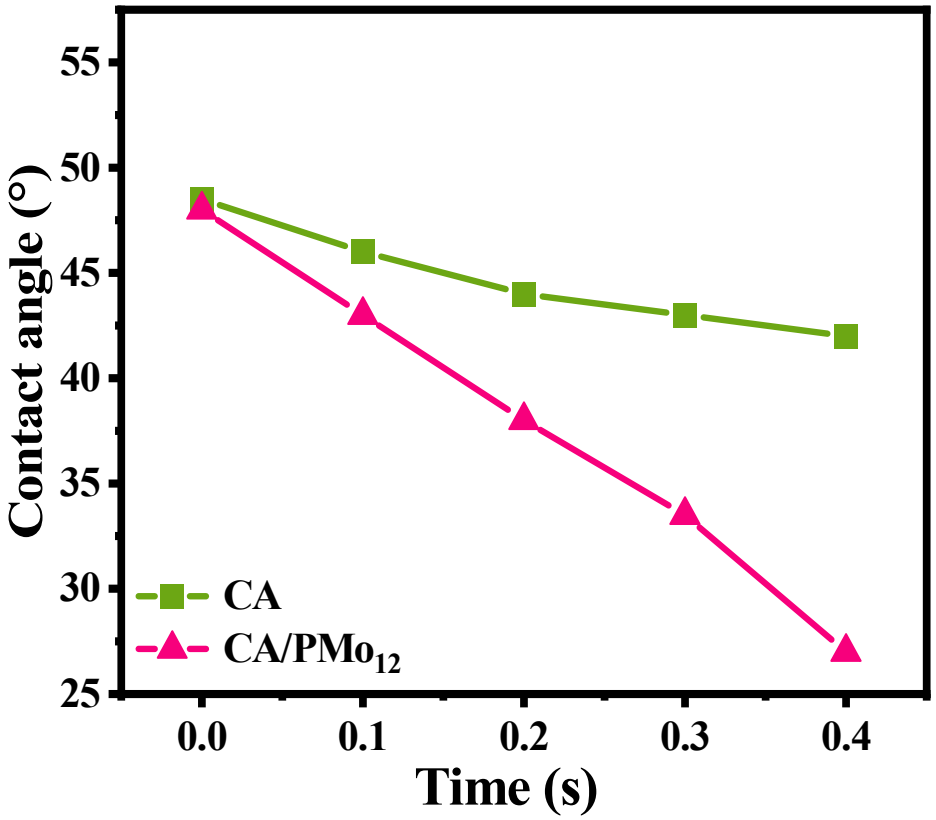

Fig. S7 The trending variations in electrolyte contact angle measurements for CA separator and CA/PMo_{12} separator.

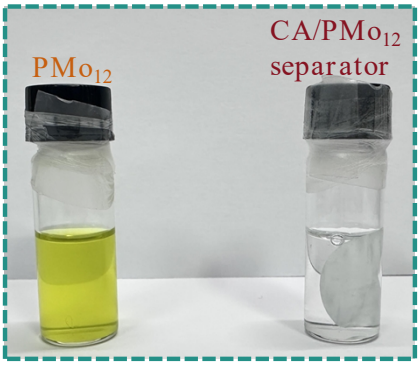

Fig. S8 Observation of solubility of PMo_{12} powder and CA/PMo_{12} separator in electrolyte (1.0 M $LiPF_6$ dissolved in DMC: EC: DME = 1: 1: 1 vol% with 10% FEC and 2% VC) after 24 h.

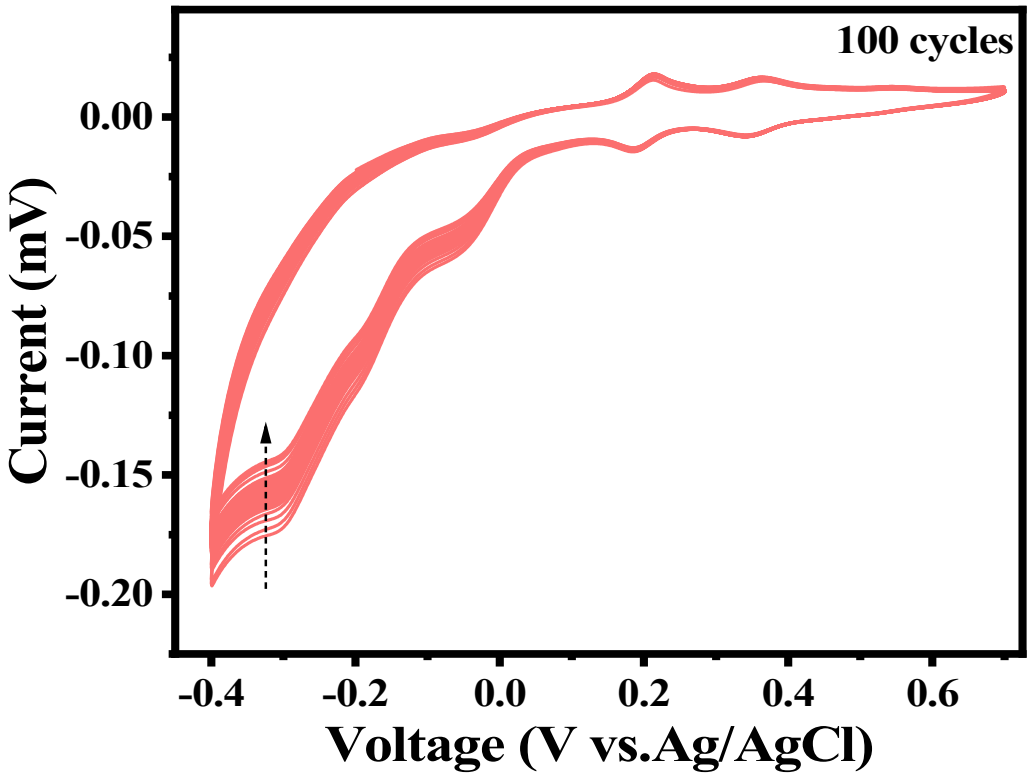

Fig. S9 CV curves of PMo_{12} at a scan rate of 0.1 V s^{-1}, and the three-electrode cell is used to test CV curves. The glass carbon electrode (5 mm in diameter), platinum wire, and the saturated Ag/AgCl electrode are employed as the working, counter, and reference electrodes, respectively.

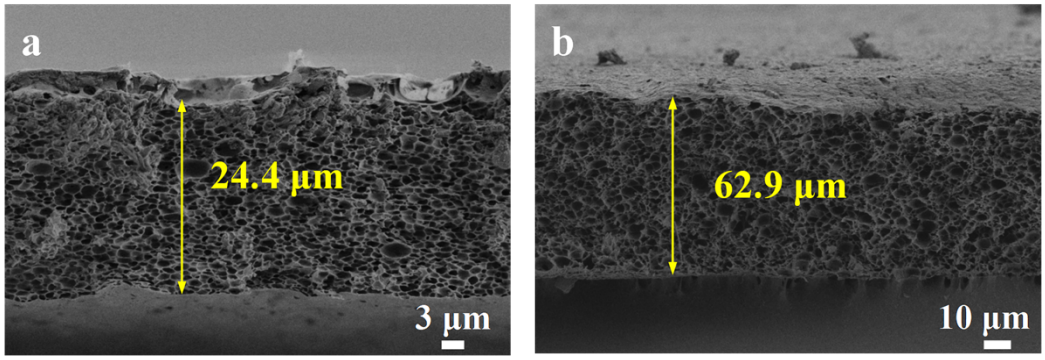

Fig. S10 The cross-section SEM images of CA/PMo_{12} separator with different thicknesses: (a) 24.4 μm and (b) 62.9 μm.

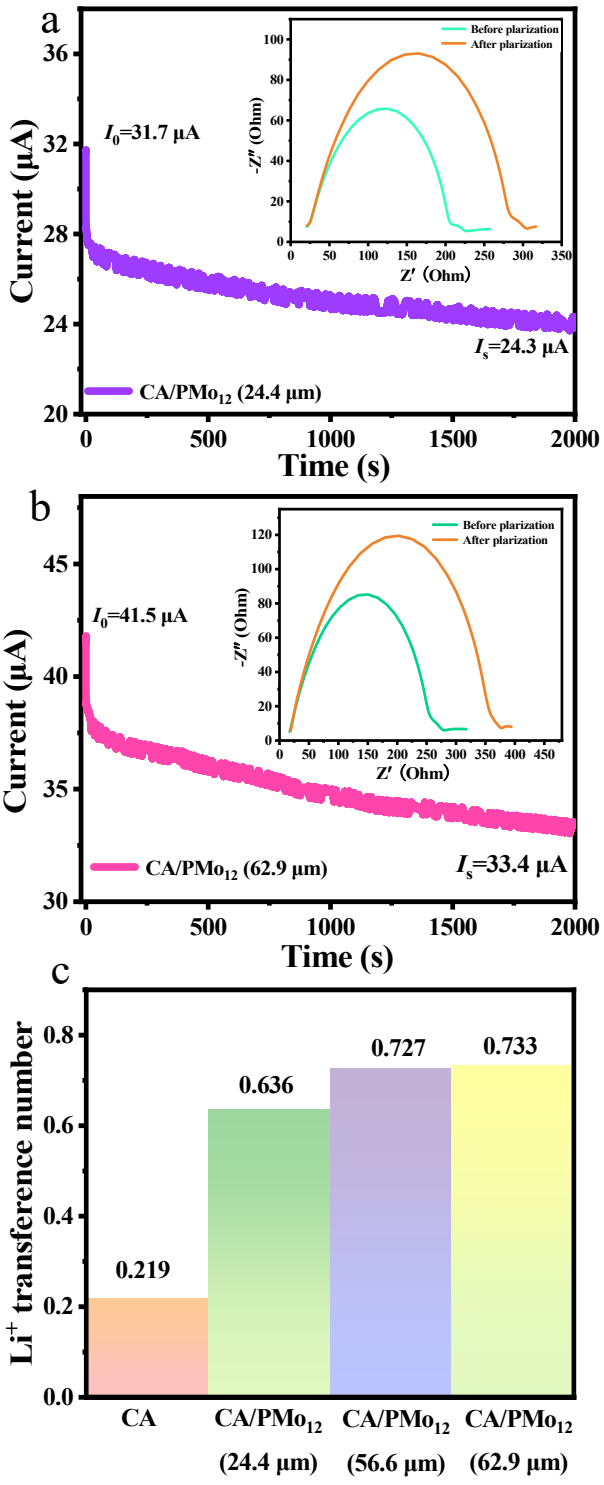

Fig. S11 (a-b) Measurement of t_{Li^+} of Li//Li symmetric cells using CA/PMo_{12} separators with different thicknesses (inset: Nyquist plots of impedance before and after polarization). (c) The values of t_{Li^+} for cells using CA/PMo_{12} separators with different thicknesses.

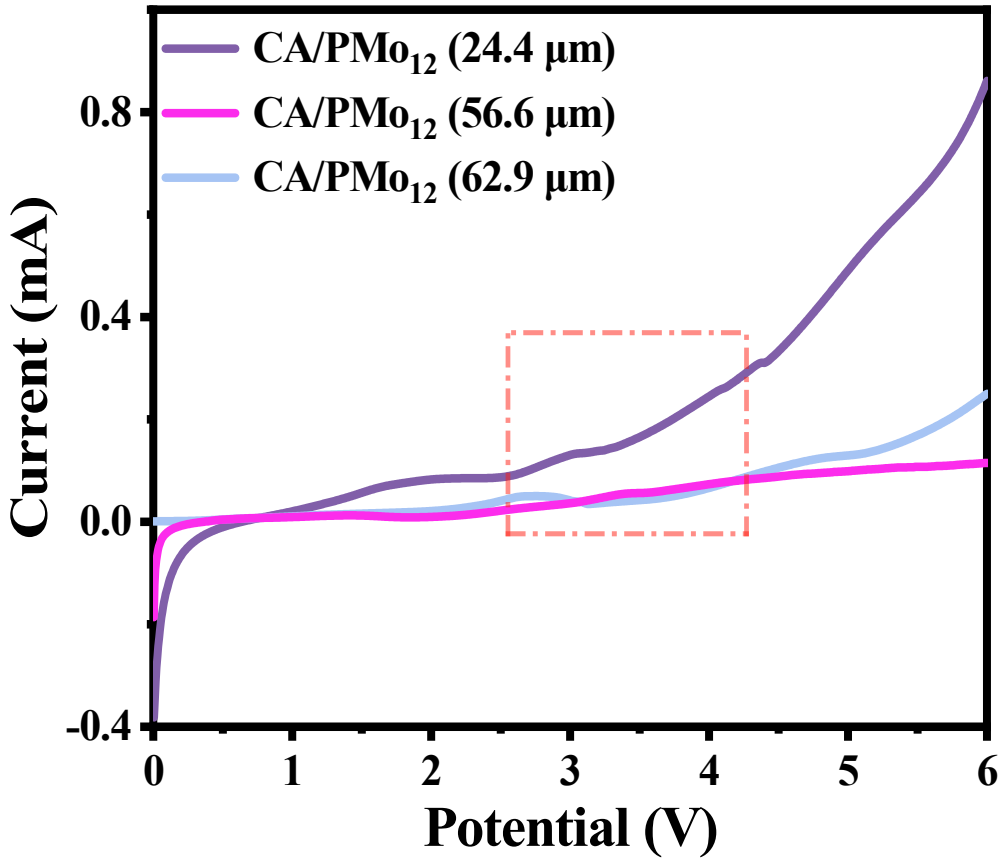

Fig. S12 LSV curves of SS//separator//SS cells using CA/PMo_{12} separators with different thicknesses.

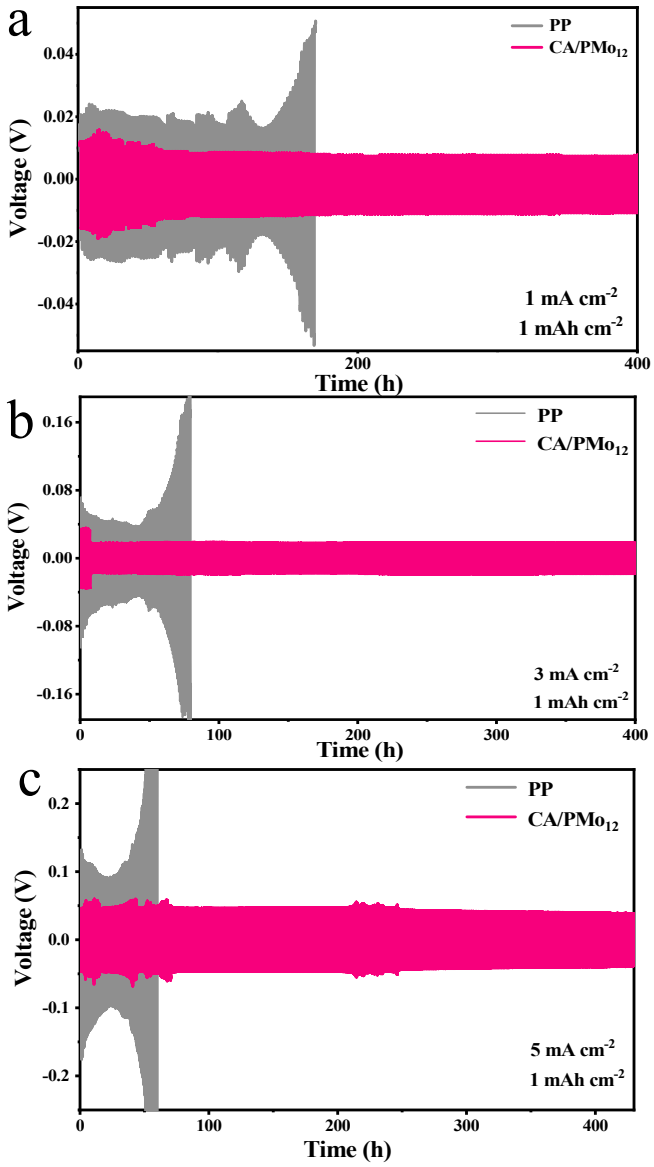

Fig. S13 (a) Galvanostatic cycling of Li//Li symmetric cells with PP and CA/PMo_{12} separators at 1 mA cm^{-2} with areal capacity of 1 mAh cm^{-2}. Galvanostatic cycling of Li//Li symmetric cells with PP and CA/PMo_{12} separators at (b) 3 mA cm^{-2} and (c) 5 mA cm^{-2} with areal capacity of 1 mAh cm^{-1}.

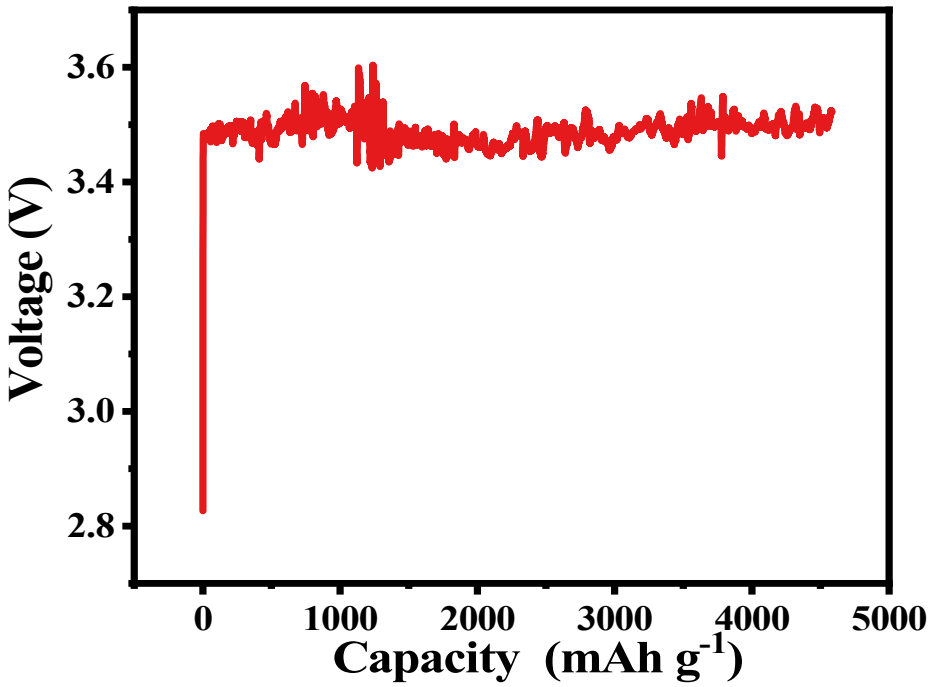

Fig. S14 The galvanostatic charge curve of $LiFePO_4$//Li cell with CA separator in the 20th cycle at 1 C.

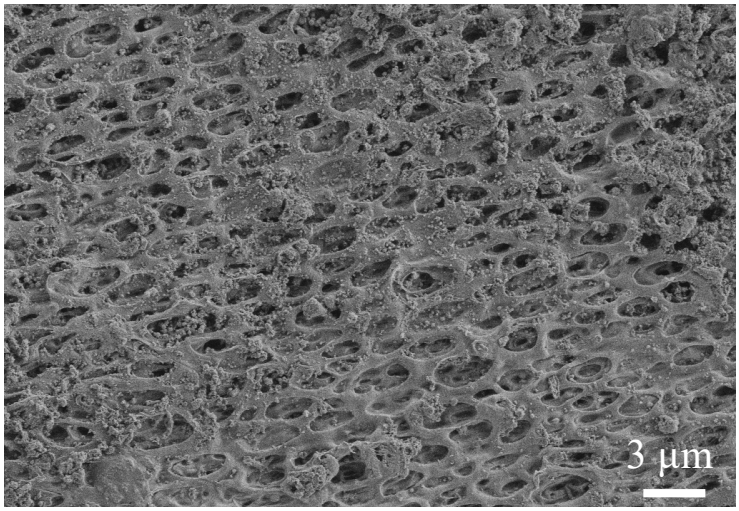

Fig. S15 SEM image of CA/PMo_{12} separator in $LiFePO_4$//Li cell after cycling.

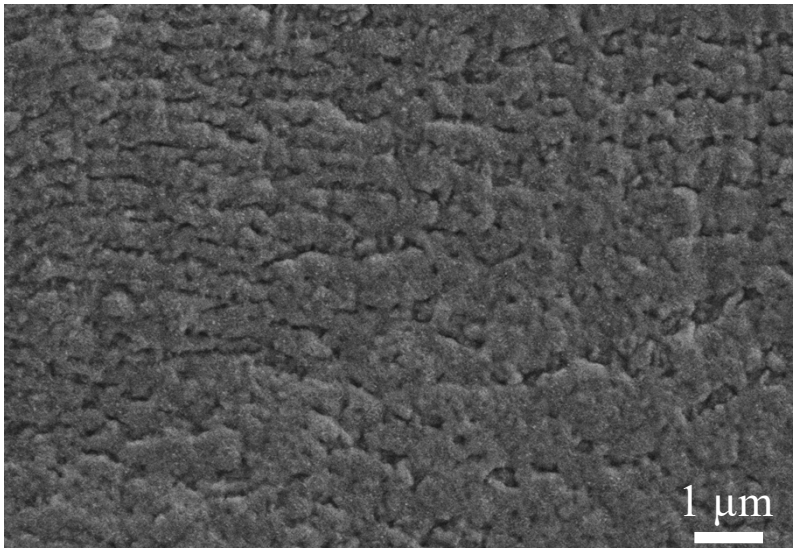

Fig. S16 SEM image of pristine lithium foil.